Over-The-Air Evaluation of 28GHz 256-Element Tiling Phased Array Antenna Module

Lei Xu,[1] Fabrício Dourado,[2] Takahito Shoji,[1] and Yujiro Tojo[3]

Millimeter-wave based technology, capable of transmitting large amounts of data in real-time with low latency and high speed, is expected to play a significant role in the fifth-generation (5G) mobile communication systems. We are developing a 28 GHz band Phased Array Antenna Module (PAAM) 「FutureAccess™」 for the 5G applications. Compared to previous PAAM, 64-element and 256-element Type-C PAAM have improved the balance between high output power and high-quality millimeter-wave signals. In this paper, we report on the performance evaluation of a 64-element PAAM and a 256-element tiled Type-C PAAM through Over-he-Air (OTA) testing.

1. Introduction

The fifth-generation (5G) networks demand faster, higher-capacity, and lower-latency communications compared to the existing fourth-generation Long Term Evolution (4G LTE) networks. With the advancement of Artificial Intelligence (AI), there is an anticipated increase in demand for high-speed communication of large-volume data in data centers and similar environments, and this demand is expected to grow similarly in wireless communications. To meet such wireless communication needs, the utilization of millimeter-wave (mmWave) frequencies is being considered in 5G networks (Figure 1). The millimeter-wave frequency band can provide a wide bandwidth, enabling the large-capacity communications required by 5G networks. However, the millimeter-wave frequency band experiences greater loss compared to lower frequency bands, resulting in a narrower coverage area[1)2)].

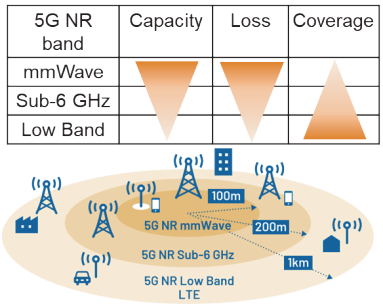

Fig. 1. 5G network.

To overcome the signal attenuation caused by such high losses, phased array antennas are employed. Since millimeter waves have shorter wavelengths compared to conventional radio frequencies, antenna elements can be made smaller, allowing these elements to be densely arranged on a planar array antenna within a compact electronic board size. Through beamforming, transmission and reception signals can be dynamically concentrated toward specific directions, thereby expanding the coverage area. Furthermore, interference from other signal sources can be suppressed by dynamically adjusting the phase and amplitude of individual antenna elements, canceling unwanted signals, and improving the overall system performance[3)].

We began development of Phased Array Antenna Modules (PAAMs) applicable to the n257, n258, and n261 bands in 2019. As shown in Figure 2, PAAMs feature high-quality signal output, high-speed beam switching, and high-precision beam control, making them suitable for use in 5G base stations, fixed wireless access (FWA), and repeaters. Currently, we have started offering the second-generation product (Type-C PAAM)[4)].

This paper reports the performance evaluation results of the FutureAccess™ Type-C PAAM based on Over-The-Air (OTA) testing.

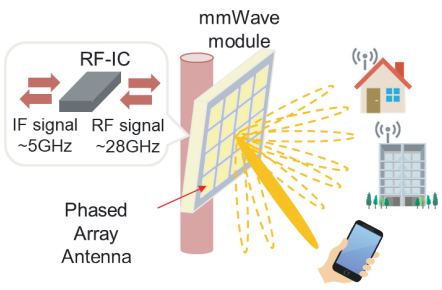

Fig. 2. Beamforming.

1 : Millimeter-wave Device Research Department, Electronic Technologies R&D Center
2 : Rohde & Schwarz GmbH & Co., KG Application Development Test and Measurement
3 : Technical Marketing Department, R&D Strategy Center

Abbreviations, Acronyms, and Terms.

5G—The fifth generation mobile communication systems
Generic term for the fifth generation communication technology.

PAAM—Phased Array Antenna Module
Antenna modules opreating phase-controlled signals simultaneously from each antenna element and working as a larger antenna that has higher gain and directivity.

RF—Radio Frequency
Frequency after up-convertion or the transmitted signal frequency.

IF—Intermediate Frequency
A frequency to which a carrier wave is shifted as an intermediate step in transmission or reception or frequency after down-conversion.

BFIC—Beamformer IC
IC to control amplification and phase-shift of transmitted and received signals.

FCIC—Frequency Converter IC
IC to perform up/down-conversion of IF signals and RF signals respectively.

COMB-SPLIT—Combiner / Splitter
Components for combining and splittting RF power while receiving and transmitting respectively.

BPF—Band Pass Filter
Components for suppressing spurious emissions.

OTA test—Over-The-Air test
Tests for evaluating transmit / receive performance and reliability of wireless devices and their antennas and other components.

Millimeter wave—Millimeter wave
The electromagnetic waves with wavelengths of 1–10 mm and frequencies of 30–300 GHz, including the frequency bands of 24.25–52.6 GHz used in 5G.

Beam Forming—Beam Forming
Technology to enhance radio wave directivity in a specified direction.

BS—Base station
A type of radio station established on land that does not move and is set up to communicate with land mobile stations.

FWA—Fixed Wireless Access
A wireless communication standard that enables broadband communication between fixed outdoor devices.

Repeater—Repeater
A wireless repeater that amplifies radio signals from a base station.

RFIC—Radio Frequency Integrated Circuit
General term for integrated circuits (ICs) that process radio frequency (RF) signals.

3GPP—Third Generation Partnership Project
A project by national standardization bodies that examines and coordinates specifications for standards for mobile communication systems beyond 3G.

n257, n258, n261 —n257, n258, n261
n257 (26.50-29.50 GHz), n258 (24.25-27.50 GHz), n261 (27.50-28.35 GHz) bands used in 5G NR.

Tx—Transmitter
A circuit that accepts signals or data in and translates them into a form that can be transmitted, usually over a distance.

Rx—Receiver
A circuit that accepts signals from a transmission medium and decodes or translates them into a form that can drive local circuits.

H pol. , V pol.—H-polarization, V-polarization
Radio waves whose plane of orientation of the electric field is horizontal (H pol.) or vertical (V pol.) with respect to the ground.

EIRP—Effective Isotropically Radiated Power
Equivalent power radiated from an isotropic directivity device producing the same field intensity at a point of observation as the field intensity radiated in the direction of the same point of observation by the discussed device.

Horn antenna—Horn antenna
A pyramidal horn antenna of known gain.

FE—Front-End
The circuit section of the antenna-side transmitter and receiver terminals.

OFDM—Orthogonal Frequency Division Multiplexing
a digital modulation technique that divides a wide frequency band into multiple closely spaced subcarriers. Each subcarrier carries a separate data stream, allowing efficient and reliable transmission, especially in environments with multipath interference.

Bandwidth—Bandwidth
Referring to the range of frequencies within a given frequency spectrum that a communication channel or signal occupies.

256QAM—256Quadrature Amplitude Modulation
A type of quadrature amplitude modulation (QAM) that uses 256-symbol constellations to transmit 8 bits at a time.

EAC—Electromagnetic Anechoic Chamber
A specially shielded laboratory that is protected from external electromagnetic waves, prevents electromagnetic leakage to the outside, and minimizes internal electromagnetic reflections.

HPBW—Half Power Beam Width
The angular width measured at the points on the main lobe of an antenna radiation pattern where the signal power drops to half of its peak value (-3 dB).

CW—Continuous Wave
An electromagnetic wave of constant amplitude and frequency that is emitted continuously over time.

LO—Local Oscillator
an electronic oscillator used in radio receivers and transmitters to generate a stable frequency signal. The signal is mixed with the incoming radio frequency signal to produce an intermediate frequency (IF) or to convert the signal to a different frequency for easier processing.

SG, VSG—Signal generator, Vector signal generator
Also known as a signal generator or vector signal generator, it is an electronic measuring instrument that outputs electrical signals with specified frequency, power, and modulation. It is used as a test signal source for radios and receivers.

SA—Signal Analyzer
Also called a signal analyzer, it is a measuring instrument that separates the individual frequency components of an input signal, displaying frequency on the horizontal axis and amplitude on the vertical axis.

Test model—Test model
A predefined signal that describes the setup of 5G NR physical channels.

IMD—Intermodulation distortion
Called intermodulation distortion, it is the distortion that occurs when multiple signals are applied to a nonlinear circuit.

EVM—Error Vector Magnitude
A quantitative measure of the difference between an ideal waveform and a measured waveform, serving as an indicator of the quality of a digital modulated signal.

ACLR—Adjacent Channel Leakage Ratio
Called Adjacent Channel Leakage Power Ratio (ACLR), it is the ratio of unwanted leakage signal power into adjacent channels in the radio frequency spectrum.

CP—Cyclic Preflix
A guard interval used to improve signal reliability in multipath environments.

OTA beam switching time—Beam switching
The time from digital signal input to beam direction change in OTA measurements.

Beam switching periodicity—Beam switching periodicity
The period at which the beam direction can be continuously switched.

True Time Delay—The true-time-delay circuit
A method of phase shifting using delay lines. In our BFIC phase shifter, the delay line is divided into sections, and by changing the inductance (L) and capacitance (C) of each divided line, the amount of delay (phase shift) can be controlled.

DDPD—Direct Digital Pre-Distortion
An iterative process that applies correction values to ensure the output signal is linear with respect to the input signal.

NTN—Non-Terrestrial Network
A network system that uses satellites or unmanned aerial vehicles to cover areas outside the range of terrestrial communication base stations.

SCS—Sub-Carrier Spacing
In multi-carrier transmissions such as OFDM (Orthogonal Frequency Division Multiplexing), it refers to the spacing between individual carriers that transmit the signal. For FR2 (28 GHz band), the subcarrier spacing is 60 kHz, 120 kHz, or 240 kHz (only for a bandwidth of 400 MHz).

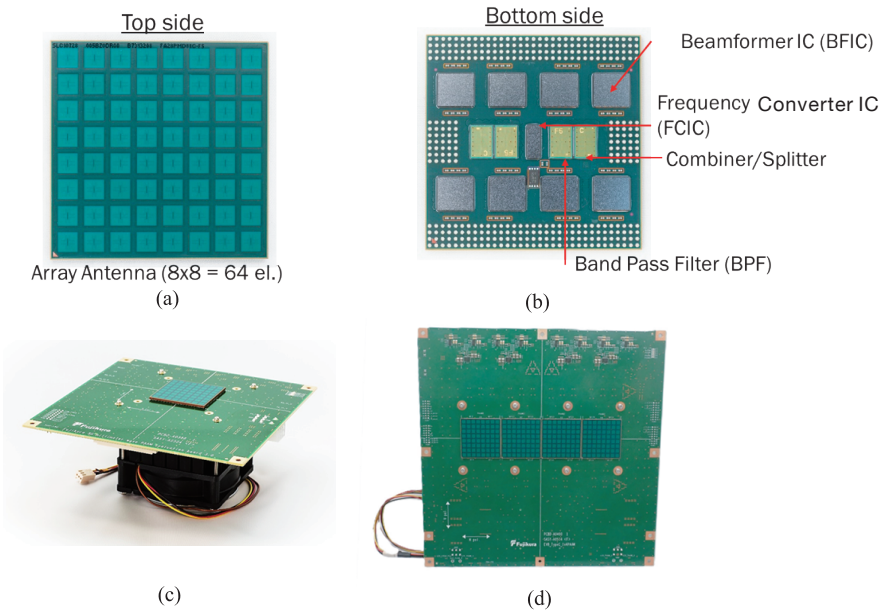

Fig. 3. Appearance of PAAM and Evaluation Board.

2. Overview

Figure 3(a) shows the antenna surface of the Type-C PAAM. The module's external dimensions are 4.25 cm × 4.25 cm, and it operates in the Third Generation Partnership Project (3GPP)-defined n257 band (26.50–29.50 GHz), n258 band (24.25–27.50 GHz), and n261 band (27.50–28.35 GHz). The antenna section employs magneto-electric dipole antennas[5] and consists of 64 elements arranged in an 8×8 array. Two types of products have been developed for the n257 and n258 bands, each covering a wide bandwidth of approximately 3 GHz.

Figure 3(b) shows the bottom side of the Type-C PAAM. One Frequency Converter IC (FCIC) is placed at the center of the module, responsible for mutually converting the Intermediate Frequency (IF) signals input/output to the PAAM and the Radio Frequency (RF) signals. To remove unwanted signals generated by frequency conversion in the FCIC, 2 Band Pass Filters (BPFs) are implemented on both sides of the FCIC. Additionally, 2 Combiner/Splitters that synthesize and distribute the filtered RF signals are positioned on both sides of the BPFs. 8 Beamformer ICs (BFICs) are installed on the PAAM. Each BFIC includes components such as phase shifters and variable gain amplifiers for 8 front-end with each polarization (16 front-end in total), controlling the phase and amplitude of the RF signals. Consequently it performs beamforming using 64 antenna elements.

Figure 3(c) shows the evaluation board equipped with the Type-C PAAM. This board includes a step-down DC-DC converter that generates 1.2 V, 1.5 V, 1.8 V, and 2.7 V from a 12 V input voltage to supply power internally. Furthermore, the internal wiring from the FCIC to the BPF, Combiner/Splitter, BFIC, and antenna is designed to be equal length for each front-end, minimizing phase variation between antennas. Also, the BFIC has been developed by utilizing true-time-delay circuit, which exhibit extremely small phase fluctuations relative to amplitude, and small amplitude fluctuations relative to phase (phase-gain orthogonality). These design features enable the PAAM to achieve high-precision beamforming control without requiring phase calibration.

Figure 3(d) shows an evaluation board tiled with four Type-C PAAMs arranged in a horizontal line. This configuration not only quadruples the number of ICs but also increases the number of antennas, enhancing directivity and improving power density as 16 times, making it suitable for longer-distance transmission.

2.1 Estimation of Transmission Speed

The transmission speed can be theoretically calculated using the following equation (1)[6].

$$\text{Data rate [bps]} = N_{mimo} \times N_{mod} \times f \times R_{max} \times (N_{RB} \times 12/T_{symbol}) \times (1 - R_{OH}) \times R_{DL/UL} \quad (1)$$

N_{mimo}: Maximum number of Multiple Input Multiple Output (MIMO) layers
N_{mod}: Number of bits per modulation symbol
f: Scaling factor (set to 1 in this case)
R_{max}: Maximum code rate
N_{RB}: Number of resource blocks per 1 Component Carrier (CC)
T_{symbol}: Duration of one Orthogonal Frequency Division Multiplexing (OFDM) symbol
R_{OH}: Overhead ratio per radio frame (0.2 for millimeter wave)
$R_{DL/UL}$: Allocation ratio of uplink to downlink in Time Division Duplex (TDD)

For example, in the case of a millimeter-wave signal with a bandwidth of 400 MHz and 64QAM OFDM, the transmission speed of a single 64-element PAAM (MIMO layer 2) is 2.52 Gbps.

By using multiple PAAMs, higher data transmission speeds can be achieved. When four PAAMs operate independently (MIMO layer 8), the transmission speed reaches 10.08 Gbps.

2.2 Test Environment

The test environment was constructed inside a large electromagnetic anechoic chamber as shown in Figure 4(a). The interior of the chamber is fully covered with mmWave compatible radio wave absorbers and shielding materials, effectively attenuating reflected waves. Inside the chamber, the PAAM evaluation board was placed on a two-axis rotary stage, and a horn antenna was positioned facing the PAAM. The required equipment was placed near either the PAAM or the horn antenna, and tests were conducted with the chamber door completely sealed. Operation of the equipment was performed remotely from outside the chamber.

2.2.1 Basic Characteristic Evaluation Using Continuous Wave

As illustrated in the OTA block diagram in Figure 4(b), the basic characteristics of the PAAM were evaluated using continuous wave (CW) signals. R&S®SMW200B signal generator (SG) was used to input the local oscillator (LO) signal to the PAAM. Additionally, R&S®SMW200A vector signal generator (VSG) was used to input the intermediate frequency (IF) signal to the PAAM. The millimeter-wave RF signal processed inside the PAAM was radiated into space. The propagated RF signal was received by the horn antenna on the opposite side, and the RF signal was evaluated by using R&S®FSW signal spectrum analyzer. In this evaluation, the received signal power measured by the FSW was converted to Effective Isotropic Radiated Power (EIRP) using a modified Friis transmission equation[7] as shown in Equation (2) below, and the radiation intensity in each direction was assessed.

$$EIRP\ (dBm) = P_R\ (dBm) - Ls\ (dB) - G_M\ (dBi) + FSPL\ (dB) \quad (2)$$

where P_R is the received power measured by the FSW, Ls is the coaxial cable loss connected to the horn antenna, G_M is the horn antenna gain, and FSPL is the Free-Space Path Loss.

2.2.2 Signal Quality Evaluation Using Modulated Signals

Signal quality was evaluated by measuring Error Vector Magnitude (EVM) and Adjacent Channel Leakage Ratio (ACLR) using 3GPP-defined modulated signals[8] (Test model 3.1a and Test model 1.1). EVM is calculated from the vector difference between the measured signal and the ideal signal, expressed as a percentage, lower EVM indicates better signal quality. In the Type-C PAAM, optimization of the level diagram between the BFIC and FCIC improved nonlinear characteristics of the signal, resulting in favorable EVM and ACLR performance.

5G NR employs the OFDM method. Depending on the IC's amplification performance, the amplitude distortion of OFDM caused by intermodulation distortion (IMD) can increase noise and degrade EVM. ACLR degradation can be also notable. 3GPP specifies measurement of EVM and ACLR using TM3.1a and TM1.1 signals, respectively, with limits set at 4.5% or less for EVM and -25.7 dBc or less for ACLR[8].

2.2.3 Confirmation of Beam Rise Time and Switching Time

High-speed beam switching is essential for reliably delivering large amount of data to multiple terminals. The Cyclic Prefix (CP) exists between symbols in the 5G New Radio (5G NR) OFDM data frame. When using a 240 kHz Subcarrier Spacing (SCS), its duration is very short at 0.29 μs[9]. Furthermore, beam switching is required to occur within 80% of the CP duration[10]. The beam switching time of the PAAM, including the digital signal instruction time to the IC, was confirmed using an oscilloscope (R&S®RTP).

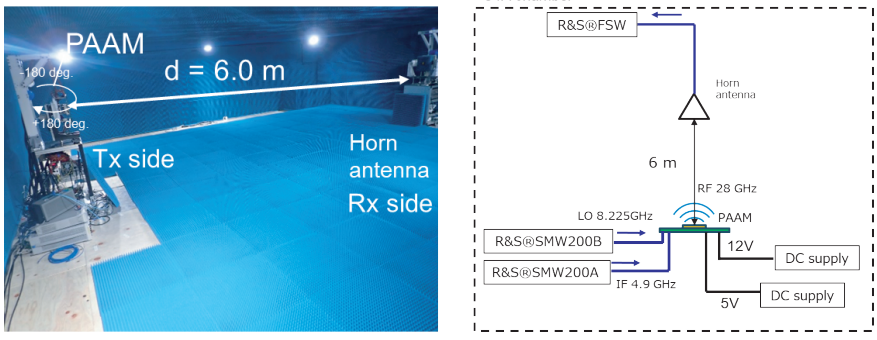

(a) (b)

Fig. 4. Test environment and measurement block diagram.

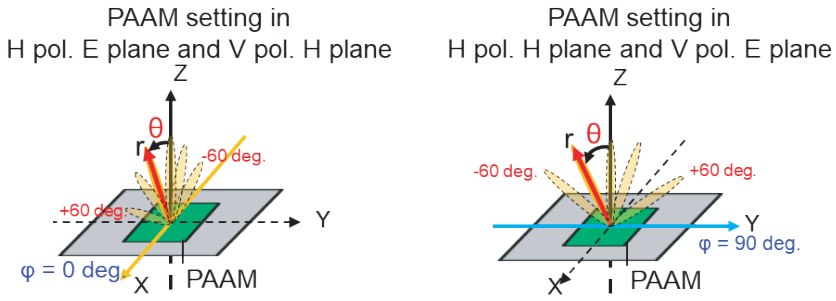

Fig. 5. Definition of beam direction from PAAM.

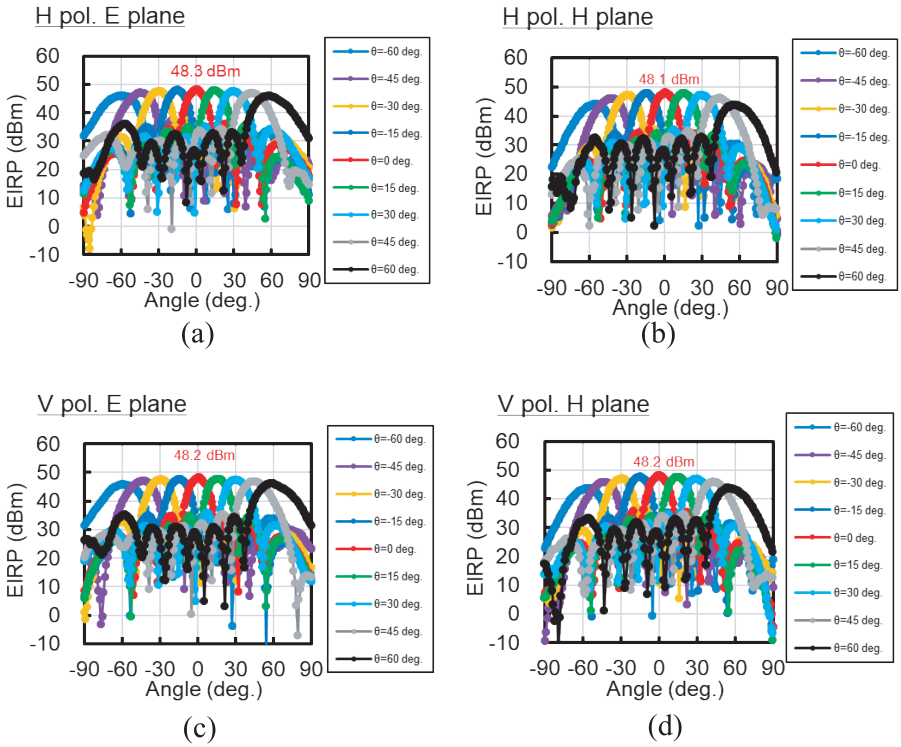

Fig. 6. Beam patterns of 64 elements PAAM.

3. Test Results

3.1 Results for 64-Element Type-C PAAM

3.1.1 Beam Pattern of the 64-Element PAAM

In these tests, the Local Oscillator (LO) frequency and Intermediate Frequency (IF) were 8.225 GHz and 4.9 GHz, respectively, producing an Radio Frequency (RF) signal at 28 GHz. The beams from the PAAM were horizontal polarization (H pol.) and vertical polarization (V pol.). The beam radiation direction θ from the PAAM was defined relative to the horn antenna's electric field plane (E plane) and magnetic field plane (H plane) as shown in Figure 5. The beam patterns were acquired by setting θ from -60° to +60° at 15° intervals. The results are shown in Figures 6(a)–(d). For each measurement, the rotary stage holding the PAAM was moved from -90° to 90° in 1° step while reading the RF signal strength displayed on the spectrum analyzer connected to the horn antenna, thereby plotting the beam pattern shape. Generally, without phase calibration for each array, large phase variations among antenna elements cause deviations from theoretically predicted patterns[11)12)]. However, our developed PAAM demonstrated beam shapes with sufficient directional accuracy for both H pol. and V pol. even without phase calibration.

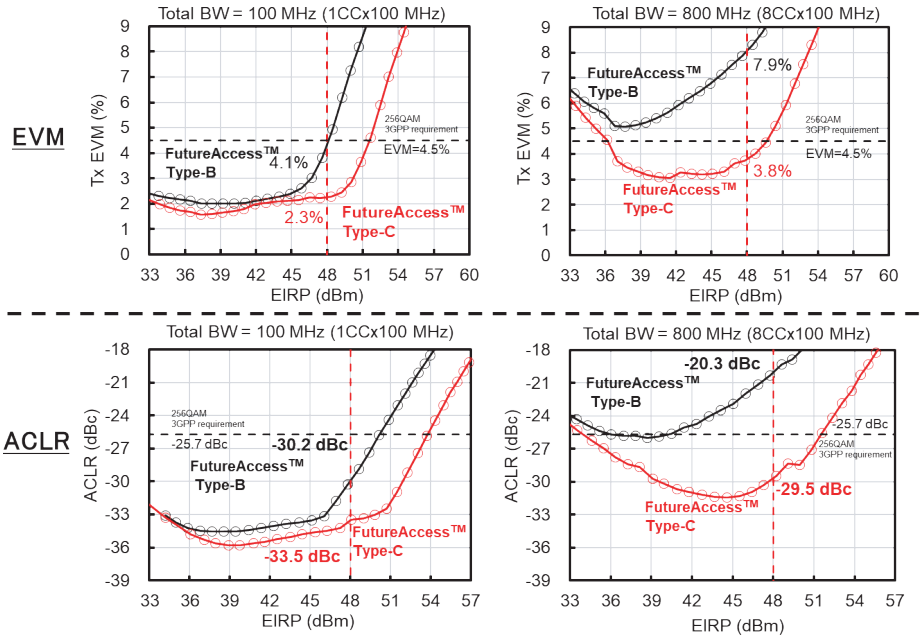

Fig. 7. EVM&ACLR results of 64 elements PAAM.

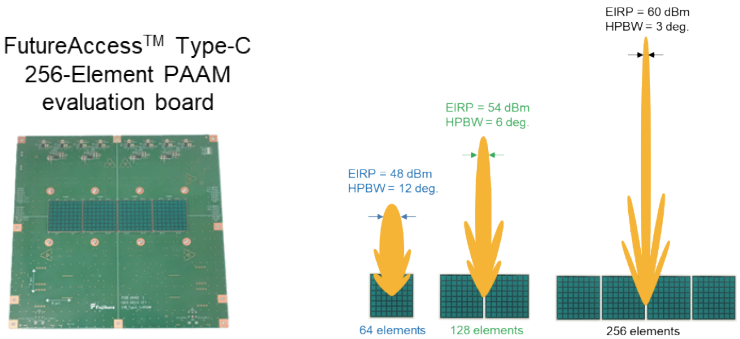

Fig. 8. Concept of PAAM tiling.

3.1.2 EVM and ACLR of the 64-Element PAAM

EVM and ACLR tests were demonstrated using 3GPP-specified test signals Test model 3.1a and Test model 1.1, respectively. The bathtub curves of EVM and ACLR versus EIRP are shown in Figure 7[13]. Compared to the previous generation PAAM, the Type-C PAAM showed significant improvement in EVM: from 4.1% to 2.3% at an EIRP of 48 dBm for 100 MHz bandwidth, and from 7.9% to 3.8% for 8 CC × 100 MHz bandwidth. Both meet the 3GPP standard of 4.5%. Similarly, ACLR improved from -30.2 dBc to -33.5 dBc for 100 MHz bandwidth, and from -20.3 dBc to -29.5 dBc for 8 CC × 100 MHz bandwidth, providing sufficient margin against the 3GPP standard of -25.7 dBc.

3.2 Results for 256-Element Tiled Type-C PAAM

3.2.1 Output Verification of the 256-Element PAAM

Figure 8 illustrates the concept of PAAM tiling. As shown in Figure 8(a), four PAAMs can be arranged in a horizontal line to create a 256-element evaluation board. Figure 8(b)[14] depicts the antenna coupling image, where increasing the number of tiled PAAMs results in narrower beamwidth and higher beam intensity. Figure 9(a) shows the relationship between the number of active elements and EIRP. While the EIRP of an 8×8 element array was 49.1 dBm, it increased to 55.1 dBm for an 8×16 element array and 60.2 dBm for a 16×16 element array. The theoretical beamforming gain obtained by increasing the element count from 64 to 256 is $20 \times \log_{10}(256/64) = 12$ dB. The experimentally obtained gain was 11.1 dB, which closely matches theoretical value, indicating effective beam combining.

Figure 9(b) shows the relationship between the number of active elements and the half-power beamwidth (HPBW). As the number of elements increases, the HPBW decreases from 12.1° for 64 elements to 3.0° for 256 elements.

3.2.2 Beam Pattern of the 256-Element PAAM

Figure 10 shows the beam patterns for the 256-element array. All beam patterns were measured without calibration. Good beam shapes were confirmed for both H pol. and V pol. Within the range of ±60°, the sidelobe

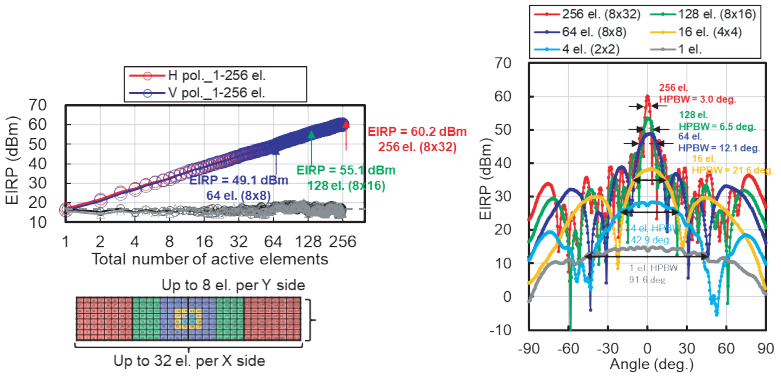

(a) (b)

Fig. 9. Relationship between active elements and output power.

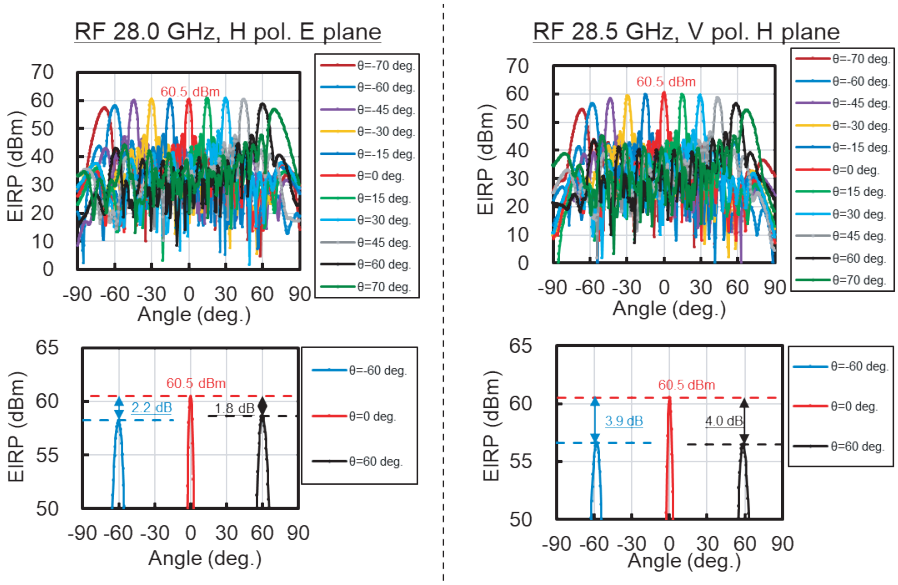

Fig. 10. Beam patterns of 256 elements.

levels were at least 11 dBc below the main lobe intensity. The variation in maximum EIRP of the main lobe across directions within ±60° was less than 4 dB.

3.2.3 EVM and ACLR of the 256-Element PAAM

The bathtub curves of EVM and ACLR relative to the PAAM's EIRP are shown in Figure 11. It was confirmed that the EIRP at 3% EVM extended by 11.2 dB compared to the 64-element Type-C PAAM. Even with the increased output power due to tiling, there was minimal degradation in signal quality. At EIRP 60 dBm, the ACLR was 29 dBc, providing approximately 3 dB of margin against the 3GPP standard of 25.7 dBc.

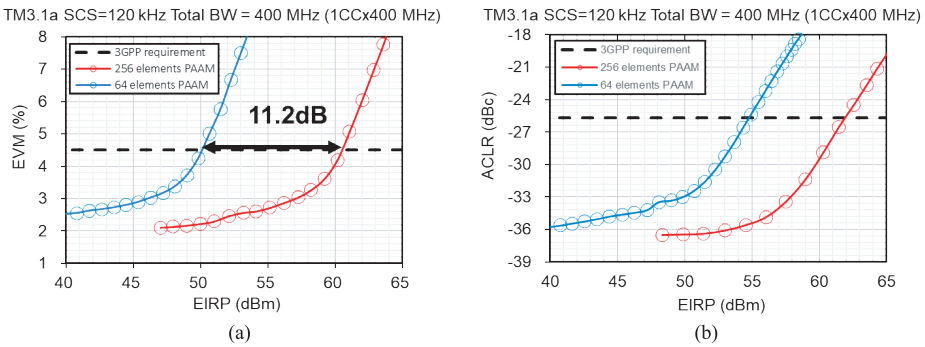

(a) (b)

Fig. 11. EVM&ACLR of 64 or 256 elements.

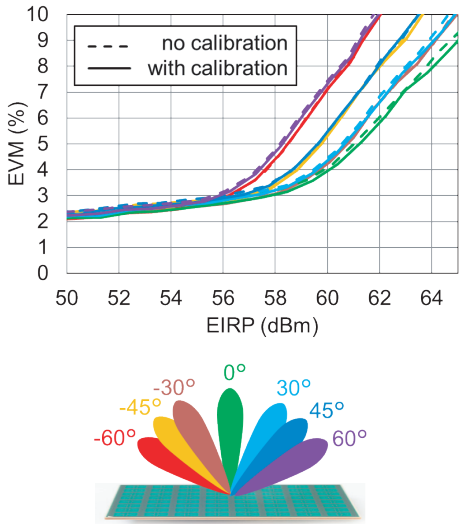

Fig. 12. EVM for each beam directions.
(The solid line shows the results with no calibration, while the dashed line shows the results with calibration. The colors in the figure correspond to the beam direction colors in the conceptual diagram at the bottom of the figure.)

Figure 12 shows the bathtub curve of EVM during beam steering within a horizontal sweep direction of ±60°. It was observed that, even without calibration, the performance was equivalent to that achieved with calibration under all beam directions.

3.2.4 Estimation of the sources of distortion in the 256-Element PAAM

This section presents the analysis results for a bandwidth of 800 MHz (8CC × 100 MHz). Using the R&S® FSW-K18[15], the sources of distortion were estimated. Generally, frequency response, noise (thermal noise or phase noise), and nonlinearity[16][17] are the factors affecting EVM. The curves in Figure 13 show the percent contribution of these factors to the mean-square-error (MSE) of non-equalized (raw) EVM measured on sample-by-sample basis. From the results, it was found that for EIRPs below 60 dBm, the nonlinear distortion of the 256-element PAAM was very low, and the primary factors affecting non-equalized raw EVM were attributed to amplitude and phase frequency responses. These results suggest that the PAAM exhibits exceptionally low phase noise and nonlinearity.

3.2.5 EVM & ACLR with DDPD

Digital predistortion (DPD) is a common method for linearizing the output signal of power amplifiers (PAs) operating in the nonlinear range[18]. Linearization typically begins with model creation, which can be challenging. By using the R&S®FSW-K18D Direct DPD (DDPD)[19], complex frequency-conversion RF Front Ends (RFFEs) can be linearized in OTA testing without a model. From a practical perspective, applying DDPD allows to verify the PAAM performance under ideal calibration and ideal linearization conditions.

Figure 14 shows the EVM and ACLR of the 256-element PAAM with and without 4.8 Gsps DDPD in combination with R&S®SMW-K555 extended bandwidth. By applying DDPD, the PAAM's EVM and ACLR at an EIRP of 60 dBm were significantly improved to less than 2% and greater than 40 dBc, respectively. These results demonstrate the full potential of the PAAM to operate with even higher power efficiency, paving the way for commercial deployment.

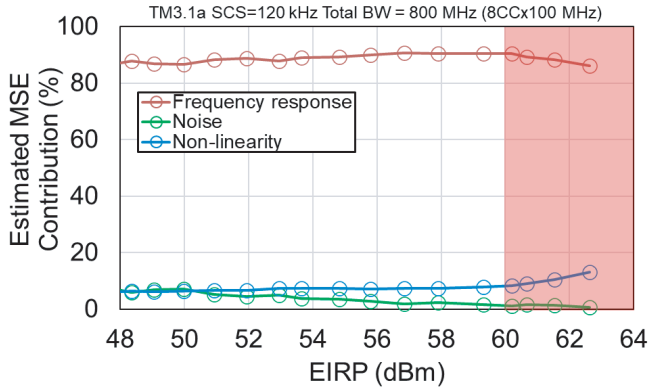

Fig. 13. Estimation of the sources of distortion in 256 elements PAAM.

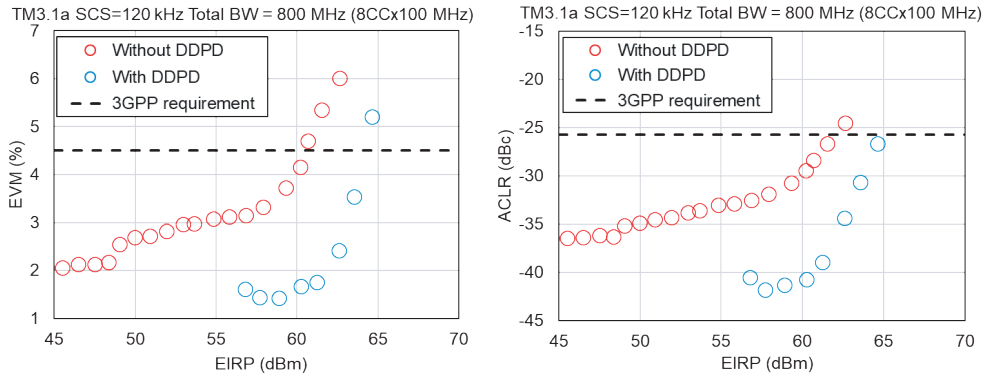

Fig. 14. EVM&ACLR of 256 elements w/wo 4.8 Gsps DDPD.

3.2.6 Fast beam switching

To observe high-speed beam switching, an oscilloscope (R&S®RTP) was used. The PAAM was digitally controlled to switch horizontal directions between 0° and 60° alternately. When the beam was directed straight to the horn antenna at θ = 0°, the signal amplitude observed on the oscilloscope was maximized. Conversely, at θ = 60°, the input power to the horn antenna significantly decreased, resulting in a minimum signal amplitude detected on the oscilloscope. The beam from the PAAM continuously moved in a sequence of 0° → 60° → 0°… The changes in the signal were measured automatically on the oscilloscope as shown in Figure 15[20]. The time between the maximum signal at θ = 0° represents the switching time from θ = 0° to θ = 60°. Including delays from analog circuits, this time was as short as 160 ns. The time from digital signal input to beam direction change was 5.4ns, approximately similar to 8 ns reported previously[4]. While the beam-switching speed should be shorter than 80% of the CP, which is 234 ns for 240 kHz, the measured beam-switching speed was much shorter, providing ample margin.

Fig. 15. Beam switching time of 256 elements PAAM.

4. Performance Comparison with Other Companies' Phased Array Antenna Modules

Table 1 shows a comparison with reported values[21-26] of silicon-based phased array antenna modules published by other companies. The main features of the PAAM developed by our company are as follows:

- Good beamforming capability for both H and V polarizations within a range of θ = ±60°
- Stable operation without calibration
- Ability to realize large antenna arrays through PAAM tiling
- Linear output range of the 64-element PAAM is EIRP = 48 dBm, and for 256 elements, EIRP = 60 dBm
- EVM and ACLR within the linear output range of the PAAM meet the 3GPP standards of 4.5% and -25.7 dBc, respectively
- Even for wideband signals with a bandwidth of 800 MHz, the PAAM achieves EVM ≤ 4.5% and ACLR ≤ -25.7 dBc at EIRP = 60 dBm
- Beam switching time is less than 220 ns, supporting more than 20,000 beam directions

5. Conclusion

We have developed a high-power PAAM for 5G communications. Through Over-The-Air testing, we confirmed that stable radiation patterns can be obtained without calibration. Additionally, by tiling 64-element PAAMs, we verified that output power can be further increased while achieving excellent modulation characteristics.

Since MIMO is required in millimeter-wave wireless base stations, we plan to evaluate the multi-beam transmission and reception characteristics and verify performance under conditions close to real environments. Furthermore, we will focus not only on ground stations but also on adaptability to Non-Terrestrial Networks (NTN), planning to assess temperature characteristics, circular polarization properties, and other relevant parameters.

Table 1. Comparison of overviews of FutureAccessTM Type-C specification and reported values of other companies [21-26].

Reported society and groups	This work	ISSCC2017 JSSC2017, IBM /Ericsson [21]	IMS2018, Qualcomm [22]	SCIS2022, Xphased Technology[23]	TMTT2021, UESTC[24]	TMTT2023, HUST [25]	IMSD2022, UCSD[26]
Chip performance comparison							
IC	130 nm SiGe	130 nm SiGe	28 nm RF	65 nm RF	180 nm SiGe	180 nm SiGe	180 nm SiGe
Technology	BiCMOS	BiCMOS	CMOS	CMOS	BiCMOS	BiCMOS	BiCMOS
Unit IC number of elements	2×8 TRX	2x16 TRX	24 TRX	2x2 TRX	2x2 TRX	8 x 4 TRX	2 x 8 TRX
Unit tile module array size	64, Dual Pol.	64, Dual Pol.	—	128, Dual Pol.	64, Single Pol.	32, Single Pol.	64, Single Pol.
Scaled tiles module array size	256, Dual Pol.	—	256, Dual Pol.	—	—	—	—
RF frequency (GHz)	24.25-29.5	27-28.5	26.5-29.5	24.25 - 29.5	23.5-29.5	26-28.5	16-50.5
IF frequency (GHz)	4.3-5.5	3	6.5	—	—	—	—
5G NR band support	Yes (n257, n258, n261)	Yes (n261)	Yes (n257, n261)	Yes (n257, n258, n261)	Yes (n257, n258, n261)	Yes (n257)	Yes (n257, n258, n259, n260, n261, n262)
Tx OP1dB (dBm)	18		—	16.8	15-16	10	13.5-14.7
Rx NF (dB)	4		—	5.5	5.5	5.5	6.2

Reported society and groups	This work	ISSCC2017 JSSC2017, IBM /Ericsson 21	IMS2018, Qualcomm22	SCIS2022, Xphased Technology 23	TMTT2021, UESTC24	TMTT2023, HUST25	IMSD2022, UCSD26
Phased array antenna performance comparison							
TX EIRP @ P1dB (dBm)	56 (64Tx) 68 (256Tx)	54 at Psat (64Tx)	35 at Psat (8TX) 64 at Psat (256Tx)	47.7 (128Tx)	54.8 (64Tx)	39 (32Tx)	64 (64Tx)
TX and RX beam scan range (deg.)	AZ ±60 EL ±60	AZ ±50 EL ±50	AZ ±45 EL ±45	AZ ±60 EL ±60	AZ ±60	AZ ±55	AZ ±60
Tx EVM (%)	≦4.5 % at EIRP 60 dBm (256Tx), 400 MHz bandwidth	—	-25 dB (5.6%) at EIRP 56 dBm, 400 MHz bandwidth	5.6% at EIRP 52.5 dBm, 400 MHz bandwidth	-26 dB (5.0%) at EIRP 47 dBm, 200MHz bandwidth	3% at 36 dBm EIRP with 64 QAM, 200 MHz bandwidth	2.90% at 36 dBm EIRP with 64 QAM, 400 MHz bandwidth
ACLR (dBc)	≦-30 dBc at EIRP 60 (256Tx) dBm, 400MHz bandwidth	—	—	—	—	—	—
Number of beams supported for fast beam-switching	> 20,000 (beam calc mode)	128	—	—	—	—	—
	2048 (beam table mode)	—	—	—	—	—	—
OTA beam switching time (ns)	＜8	4	—	—	—	—	—
Beam-switching periodicity (ns) periodicity (ns)	< 220 (including control time)	—	—	—	—	—	

References

1) Fujikura Ltd., “28 GHz Fujikura’s state-of-the-art 5G Phased Array Antenna Module: FutureAccess™”, https://mmwavetech.fujikura.jp/5g/ (Viewed on 19th Mar. 2025)
2) S. Pramono et al., “Design and Challenges on mmWave Antennas: A Comprehensive Review,” E3S Web of Conferences 465, 02067, 2023.
3) A. K. Pandey, “Phased Array Antenna with Beamforming Network,” Proceedings of the 50th European Microwave Conference.
4) https://mmwavetech.fujikura.jp/
5) B. Sadhu et al., “A 24-to-30GHz 256-Element Dual-Polarized 5G Phased Array with Fast Beam- Switching Support for >30,000 Beams”, ISSCC, February. 2022.
6) https://www.fujikura.co.jp/research/pdf/technical-report/138/138_R4.pdf
7) H.T. Friis "A Note on a Simple Transmission Formula". Proc. IRE, vol. 34, no. 5, pp 254–256, May 1946.
8) 3GPP TS 38.141-2 V17.15.0, Base Station (BS) Conformance Testing, Part 2: Radiated Conformance Testing, Sep. 2024.
9) S. Ahmadi, 5G NR: Architecture, Technology, Implementation, and Operation of 3GPP New Radio Standards. New York, NY, USA: Academic, 2019.
10) J.A. Fabien, “Channel Model Implementation and Application for New Radio (NR) 3GPP REL-15”, Institute for Telecommunication Sciences, 2018.
11) R. Hamarneh, “Analytical Calibration Scheme Suitable for Modern Mobile Communication Systems,” EECS, p34, Stockholm Sweden, 2020.
12) M. Sierra-Pereza et al., "Integration, Measurements and Calibration of A UMTS Smart Antenna". 2004 IEEE 15th International Symposium on Personal, Indoor and Mobile Radio Communications (IEEE Cat. No.04TH8754), Sep. 2004.
13) Y. Tojo "Over-The-Air test of phased array antenna module of 28 GHz band", Rohde & Schwarz Technology Symposium 2024 - Japan, Session 4 of Automotive and wireless related technologies, https://rohde-schwarz-japan.com/download/techsympo2024/AUT-WIC04_rs_techsympo2024-seminar-text.pdf
14) Y. Tojo, “Beam direction accuracy and 2D radiation antenna pattern measurements of 256 elements phased array”, THMA5, IMS2024, Washington. D.C., U.S. (2024).
15) F. Ramian, “Amplifier characterization using non-CW stimulus,” 2017 IEEE International Workshop on Metrology for AeroSpace (MetroAeroSpace), pp. 198-200, June. 2017, Padua, Italy.
16) F. Ramian, D. Tipton, “Detailed EVM, statically independent contribution to EVM,” Short Tutorial Video in the R&S Amplifier Master Class Series, Munich, Germany, June 2020, https://www.youtube.com/watch?v=v2CatcQAm7c&list=PLKxVoO5jUTlvZVUh2Gn_6BYZtAsQtUHAC&index=5
17) F. Dourado, L. Xu, “Over-the-air mmWave phased array distortion analysis and linearization testing,” IWWE3, IMS2024, Washington. D.C., U.S. (2024).
18) F. Ramian, “Iterative Direct DPD,” White Paper, Munich, Germany, Sept. 2017, http://www.rohde-schwarz.com/appnote/1EF99 https://www.rohde-schwarz.com/jp/applications/dpd-white-paper_230854-478144.html
19) S. Obernberger, S. Kehl-Waas, “Digital pre-distortion for improved EVM performance,” Application Note, Munich, Germany, Aug. 2023, https://www.rohde-schwarz.com/appnote/1GP139 https://www.rohde-schwarz.com/jp/applications/digital-predistortion-for-improved-evm-performance-application-note_56280-1401410.html
20) L. Xu et al., “How to measure beam switching speed why is it important and what is the necessary performance,” THMA5, IMS2024, Washington. D.C., U.S. (2024).
21) B. Sadhu et al., “A 28GHz 32-Element Phased-Array Transceiver IC with Concurrent Dual Polarized Beams and 1.4 Degree Beam-Steering Resolution for 5G Communication”, ISSCC, pp. 128-129, Feb. 2017.
22) J. Pang et al., “A 28-GHz CMOS Phased-Array Beamformer Utilizing Neutralized Bi-Directional Technique Supporting Dual-Polarized MIMO for 5G NR”, IEEE JSSC, vol. 55, no. 9, Sep. 2020.
23) H. Liu et al., “A 24.25–27.5 GHz 128-element Dual-polarized 5G integrated Phased Array with 5.6%-EVM 400-MHz 64-QAM and 50-dBm EIRP”, Sci China Inf Sci, vol. 65, 214401:1-3, Nov. 2022.
24) Y. Yin et al., “Wideband 23.5–29.5-GHz Phased Arrays for Multistandard 5G Applications and Carrier Aggregation”, IEEE TMTT, vol. 69, no. 1, Jan. 2021.
25) S. Wang et al., “Dual-Band 28- and 39-GHz Phased Arrays for Multistandard 5G Applications”, TMTT, vol. 71, no. 1, Jan. 2023.
26) A. Alhamed et al., “16-52 GHz 5G Transmit and Receive 64-Element Phased-Arrays With 50-51.7 dBm Peak EIRP and Multi-Gb/s 64-QAM Operation”, IEEE/MTT-S, Jun. 2022.